# Quantum metrology timing limits of the Hong-Ou-Mandel interferometer and of general two-photon measurements

Kyle M. Jordan [1,*] Raphael A. Abrahao [1,2] and Jeff S. Lundeen [1,3]

[1]*Department of Physics and Center for Research in Photonics, University of Ottawa,*
25 Templeton Street, Ottawa, Ontario, Canada K1N 6N5
[2]*Brookhaven National Laboratory, Upton, New York 11973, USA*
[3]*Joint Center for Extreme Photonics, University of Ottawa and National Research Council of Canada,*
100 Sussex Drive, Ottawa, Ontario, Canada K1A 0R6

We examine the precision limits of Hong-Ou-Mandel (HOM) timing measurements, as well as precision limits applying to generalized two-photon measurements. As a special case we consider the use of two-photon measurements using photons with variable bandwidths and frequency correlations. When the photon bandwidths are not equal, maximizing the measurement precision involves a tradeoff between high interference visibility and strong frequency anticorrelations, with the optimal precision occurring when the photons share nonmaximal frequency anticorrelations. We show that a generalized measurement has precision limits that are qualitatively similar to those of the HOM measurement whenever the generalized measurement is insensitive to the net delay of both photons. By examining the performance of states with more general frequency distributions, our analysis allows for engineering of the joint spectral amplitude for use in realistic situations, in which both photons may not have ideal spectral properties.

I. INTRODUCTION

In the Hong-Ou-Mandel (HOM) effect, two photons incident on both input ports of a 50:50 beam splitter, identical in all degrees of freedom, will both emerge from the same output port [1,2]. Conversely, a reduction in the HOM effect may be used to estimate differences in the photon properties, allowing for its use as a sensor. This behavior forms the foundation of many technologies of current interest, being used in optical quantum logic gates [3], in the characterization of single-photon sources [4], in measurements of the quantum tunneling time [5], for fundamental tests of quantum nonlocality [6], and as a tool for precise measurement of time delays [1,7,8], of spatial shifts [9], and of frequency shifts [10]. The experimental implementation of HOM-based measurement schemes is also simplified by the use of fast single-photon-sensitive detector arrays, as demonstrated by Ref. [11]. The application to precision measurements has been known since the initial investigations into the HOM effect [1]. Despite this, it is only recently that rigorous studies of the fundamental precision limits of HOM interferometry have been undertaken, spurred in part by experiments [7,8] demonstrating few-attosecond timing (nanometer path length) precision.

Questions about the fundamental precision limits of physical measurements are answered by the methods of quantum metrology. These theoretical tools place bounds on the precision of any physical measurement allowed by the laws of quantum mechanics [12,13]. Quantum metrology has typically focused on improving the resolution of phase-sensitive interferometers, through techniques such as quadrature squeezing [14] and N00N state interferometry [15]. In noisy environments, however, it is difficult to provide the phase stability needed for these techniques. A HOM interferometer is sensitive only to the group delay of the photons rather than their phase shifts and is immune to some forms of chromatic dispersion [16], making it a promising candidate for precision measurements in noisy or dispersive environments [17].

This paper studies the theoretical precision limits applying to HOM timing measurements and to more general forms of measurement using two-photon probe states. Our analysis focuses on the classical and the quantum Fisher information, which are used to find the optimal timing precision of a particular measurement scheme and of any physical measurement, respectively. Analysis of this kind has been conducted in past work [7,8,17,18], with the key conclusion that HOM interferometry is an optimal measurement of the relative photon delay and that the precision is limited by the bandwidth of the probe photons rather than their mean wavelength. To date, these metrological studies have focused exclusively on two-photon states in which each photon has the same bandwidth and which share maximal anticorrelations in frequency. In addition, they have considered only the effect of a single unknown photon delay, when in many practical scenarios neither photon delay is known in advance. The analysis we present here addresses both of these problems, extending the previous work to include more general two-photon states as well as examining the effect of shifts in both photon delays on the precision of timing measurements.

---
*kjordan@uottawa.ca

The HOM interferometer is used in a variety of specific metrological timing-based tasks, including ranging [19], refractometry [20], and quantum-enhanced optical coherence tomography [21]. No single set of measurement parameters describes all measurements made with the technique. For the purpose of this work, we exclusively focus on those situations in which a single time delay (the relative photon delay) is to be estimated. In many situations, such as measurements of birefringence, only the relative delay between photons, $\tau_- \equiv (\tau_1 - \tau_2)/2$, is of interest, rather than the delay of a particular photon. The HOM measurement may measure τ_- precisely, but it is inherently insensitive to small shifts of the mean delay of both photons, $\tau_+ \equiv (\tau_1 + \tau_2)/2$. This may be remedied through the use of an additional timing measurement to estimate τ_+, but in many circumstances, such as clock synchronization [22], estimation of τ_+ by any means is impractical. Proper metrological bounds, such as those we present, must therefore consider the effect of the unknown delay τ_+ on the measurement precision for estimates of τ_-.

In addition, in situations such as ranging or refractometry, the two photons experience very different optical environments; one photon is typically stored in a carefully designed optical system, while the other is transmitted through an uncontrolled environment that may exhibit strong dispersion or absorption. In these situations, it is likely that measurement of the relative delay τ_- of photons with different bandwidths is necessary. The effect of unequal bandwidths must also be addressed as a source of experimental error: Nonlinear sources of photon pairs rely on birefringence to obtained the necessary phase-matching relations, so photons are naturally created in different optical environments and with different spectral properties [23]. We show that it is exactly when the photon bandwidths differ that the unknown delay τ_+ may degrade estimation of the relative delay τ_-. Under these circumstances, we show that the common wisdom of using states with highly anticorrelated frequencies does not offer the optimal precision and find certain qualitative similarities between the HOM measurement and any optimal measurement of τ_- that is ignorant of the delay τ_+. Though bulk down-conversion sources of photons naturally produce photon pairs with strong anticorrelations, this work, together with custom-engineered down-conversion sources [24,25], enables the possibility of tailoring the two-photon frequency correlations to optimize precision in these unbalanced interferometers.

We give here a theoretical analysis of the precision of measurements of the relative delay τ_- of two photons, considering more general two-photon states which may have unequal single-photon parameters. In particular, we consider the behavior of pairs where photons may have different bandwidths, different center wavelengths, and varying degrees of frequency correlations. This paper consists of two main parts. In the first part, Sec. II, we consider the precision limits applicable to measurements of the relative delay between two photons, regardless of the exact measurement scheme used. Our model places delays before any interference optics, so that it is applicable to HOM measurement, as well as modified schemes such as the spectrally resolved HOM measurement [26]. We show that in the case of unequal photon bandwidths, the precision limits for the relative photon delay depend crucially on which parameters are initially known and which
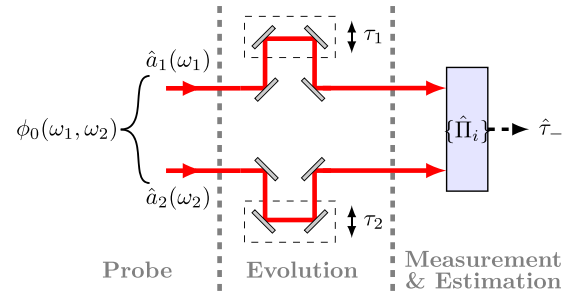

FIG. 1. General scheme for estimation of the relative photon delay $\tau_- = (\tau_1 - \tau_2)/2$ using a two-photon probe state. The probe, consisting of a single photon in each of two spatial modes ($\hat{a}_1$ and $\hat{a}_2$), undergoes delays (τ_1 and τ_2) in each arm. Measurement(s) are made (depicted by the projectors $\{\hat{\Pi}_i\}$) and the relative delay is estimated from measurement statistics.

are unknown. In the second part, Sec. III, we examine the precision limits specific to HOM interferometry. We compare the performance of the HOM measurement to the fundamental precision limits derived in the Sec. II of the paper and determine those situations in which an alternative measurement may be advantageous. A summary of our results is provided in Appendix A for easy reference.

II. QUANTUM METROLOGICAL LIMITS TO TWO-PHOTON TIMING

This section derives precision limits governing measurements of the relative delay τ_- between two photons. In Sec. II A we define the relevant metrological quantities used in this section and in our analysis of the Hong-Ou-Mandel interferometer in Sec. III and summarize the key precision bounds involving these quantities. In Sec. II B we define the two-photon probe state of interest and describe its evolution under two variable delays. In Sec. II C we give the precision limits for estimation of one photon's delay when the other photon's delay is known. Finally, in Sec. II D we consider the problem of estimating the relative delay τ_- between two photons in the presence of an unknown mean delay τ_+, providing the relevant precision limits and outlining optimal strategies in a few specific scenarios.

A. Classical and quantum estimation theory

A general measurement consists of four main steps, depicted in Fig. 1 for a two-photon timing measurement. First, a known probe state $\hat{\rho}$ is prepared; second, the state undergoes an unknown evolution parametrized by the unknown quantities $\{\theta_i\}$, leading to the postevolution state $\hat{\rho}'(\theta_i)$; third, the state is measured, leading to measurement outcomes $\{O_i\}$; finally, estimates $\{\hat{\theta}_i\}$ of one or more parameters are made. The precision of the estimates is defined to be the standard deviation $\Delta\theta_i \equiv \sqrt{\langle\Delta^2\theta_i\rangle}$ of the estimates, taken over an ensemble of identical measurements (including preparation, evolution, measurement, and estimation). Here $\langle\Delta^2\theta_i\rangle$ denotes the variance of the estimate $\hat{\theta}_i$, evaluated for the particular probe state used. The goals of quantum metrology are to find the optimal (minimum) possible values of the $\Delta\theta_i$ for a given probe state and for a given measurement.

For simplicity, we focus first on the case of a single unknown parameter θ. The metrological quantities of interest to us are then the classical Fisher information (CFI) $\mathcal{F}$ and the quantum Fisher information (QFI) $\mathcal{Q}$. Each quantity provides a distinct bound on the precision of a given measurement scheme. Given a particular probe state and measurement scheme, the classical Cramér-Rao bound (CCRB) states

$$\langle \Delta^2 \theta \rangle \geqslant \frac{1}{n\mathcal{F}} \tag{1}$$

after n repetitions of the measurement have been performed. If measurement outcome $\mathcal{O}_i$ occurs with probability p_i, then the CFI is given by the expression

$$\mathcal{F} = \sum_i \frac{(\partial p_i / \partial \theta)^2}{p_i}, \tag{2}$$

where the p_i have an implicit dependence on the particular probe state used and on the measurement scheme in question. The quantum Cramér-Rao bound (QCRB) [12] states $\langle \Delta^2 \theta \rangle \geqslant 1/n\mathcal{Q}$, where $\mathcal{Q}$ depends only on the probe state in question; the exact form of $\mathcal{Q}$ varies, depending on the type of probe and evolution in question. Since the QCRB applies to any possible measurement we have $\mathcal{F} \leqslant \mathcal{Q}$, where both quantities are evaluated for the same probe state, leading to the chain of inequalities

$$\langle \Delta^2 \theta \rangle \geqslant \frac{1}{n\mathcal{F}} \geqslant \frac{1}{n\mathcal{Q}}. \tag{3}$$

The QFI can thus be used to select an optimal probe state, while the CFI can be used to evaluate the performance of a given measurement scheme.

We turn now to the case of multiple unknown parameters $\{\theta_i\}$, focusing exclusively on the generalization of the QFI. The figure of merit for estimations of the θ_i is still the variances $\langle \Delta^2 \theta_i \rangle$, here obtained as the diagonal elements of the covariance matrix $\mathcal{C}$ of the estimates $\hat{\theta}_i$. The QCRB now takes the form [13]

$$\mathcal{C} \geqslant \frac{1}{n} \mathcal{Q}^{-1}, \tag{4}$$

with $\mathcal{Q}$ the quantum Fisher information matrix, which again depends only on the probe state in question. The diagonal elements of this inequality take the form

$$\langle \Delta^2 \theta_i \rangle \geqslant \frac{1}{n\mathcal{Q}_{\text{eff}}^{(i)}}, \tag{5}$$

similar to the single parameter QCRB. The quantities $\mathcal{Q}_{\text{eff}}^{(i)} \equiv 1/(\mathcal{Q}^{-1})_{ii}$ here play the role of an effective QFI. For two unknown quantities, indexed by $i = 1, 2$, the effective QFI takes the form

$$\mathcal{Q}_{\text{eff}}^{(1)} = \mathcal{Q}_{11} - \frac{\mathcal{Q}_{12}{}^2}{\mathcal{Q}_{22}}, \quad \mathcal{Q}_{\text{eff}}^{(2)} = \mathcal{Q}_{22} - \frac{\mathcal{Q}_{12}{}^2}{\mathcal{Q}_{11}}. \tag{6}$$

The presence of a nonzero off-diagonal term $\mathcal{Q}_{12}$ results in the multiparameter effective QFI of a given θ_i being less than the single parameter QFI of θ_i, were all other parameters known. As discussed in [13], the presence of additional unknown parameters generally reduces the measurement precision even for estimates of a single parameter of interest. This is particularly relevant to the problem of two-photon timing measurements, for which the optimal estimation precision of the relative photon delay τ_- is potentially degraded depending on whether the mean photon delay τ_+ is known in advance.

B. Two-photon probe state and evolution

We consider now the particular problem of two-photon timing estimation. The probe state of interest is a pure quantum state containing a single photon in each of two orthogonal spatial modes. Equivalently, the photons may occupy the same spatial mode, but have orthogonal polarization states. Defining $\hat{a}_1^\dagger(\omega)$ and $\hat{a}_2^\dagger(\omega)$ to be creation operators that place a photon of angular frequency ω in the first and second spatial modes, the probe state may be written in the general form

$$|\psi_0\rangle = \iint d\omega_1 d\omega_2 \phi_0(\omega_1, \omega_2) \hat{a}_1^\dagger(\omega_1) \hat{a}_2^\dagger(\omega_2) |0\rangle . \tag{7}$$

The complex function $\phi_0(\omega_1, \omega_2)$ is known as the joint spectral amplitude (JSA) and describes the entire spectral content of the state, including the bandwidths and mean frequencies of individual photons, as well as any frequency correlations or anticorrelations between the two photons. The squared quantity $|\phi_0(\omega_1, \omega_2)|^2$ is known as the joint spectral intensity. Due to the orthogonality of the two spatial modes, the creation operators satisfy $[\hat{a}_i(\omega), \hat{a}_j^\dagger(\omega')] = \delta_{ij}\delta(\omega - \omega')$. Normalization of the state $|\psi_0\rangle$ implies that

$$\iint d\omega_1 d\omega_2 |\phi_0(\omega_1, \omega_2)|^2 = 1. \tag{8}$$

Throughout our analysis, we will express quantities in terms of the probe state, using $\langle \hat{X} \rangle_0$ to denote the expectation value of the operator $\hat{X}$ for a probe state $|\psi_0\rangle$ and $\langle \Delta^2 \hat{X} \rangle_0$ to denote the variance of $\hat{X}$ for the same state.

It is useful to briefly review the properties of typical two-photon states. The most common method of producing states of this form are through $\chi^{(2)}$ nonlinear optical interactions, such as spontaneous parametric down-conversion, in which a single pump photon of energy $\hbar\omega_p$ is converted into a pair of photons of energies $\hbar\omega_s$ and $\hbar\omega_i$ [23]. Due to the requirement $\omega_p = \omega_s + \omega_i$ for energy conservation, the down-converted photons typically exhibit frequency anticorrelations, with the strength of the correlations being related to the bandwidth of the pump beam. The specific nonlinear medium used in the process enforces a phase-matching relation between the wave vectors of the pump and down-converted photons, which plays the role of momentum conservation for the system. The JSA of the resulting two-photon state is a product of the pump spectrum and a phase-matching factor. The advent of engineered nonlinear crystals, such as periodically poled media, as well as the use of broadband pump beams, allows for the generation of a variety of custom JSAs, exhibiting frequency anticorrelations, frequency correlations, and uncorrelated frequencies [24,25].

Upon evolution through the two time delays τ_1 and τ_2, as depicted in Fig. 1, the two-photon state will evolve as $|\psi_0\rangle \rightarrow |\psi(\tau_1, \tau_2)\rangle = \hat{U}(\tau_1, \tau_2)|\psi_0\rangle$, where the unitary operator $\hat{U}(\tau_1, \tau_2)$ has the form

$$\hat{U}(\tau_1, \tau_2) = \exp(-i\hat{\Omega}_1\tau_1 - i\hat{\Omega}_2\tau_2) \tag{9a}$$

$$= \exp(-i\hat{\Omega}_-\tau_- - i\hat{\Omega}_+\tau_+). \tag{9b}$$

The generators $\hat{\Omega}_1$ and $\hat{\Omega}_2$ are given by

$$\hat{\Omega}_i \equiv \int d\omega\, \omega\, \hat{a}_i^\dagger(\omega)\hat{a}_i(\omega). \tag{10}$$

Here $\hat{\Omega}_\pm \equiv \hat{\Omega}_1 \pm \hat{\Omega}_2$ act as generators of the relative delay $\tau_- \equiv (\tau_1 - \tau_2)/2$ and the mean delay $\tau_+ \equiv (\tau_1 + \tau_2)/2$. Upon evolution, the creation operators transform as $\hat{a}_i^\dagger(\omega) \rightarrow \hat{a}_i^\dagger(\omega)e^{-i\omega\tau_i}$. The postevolution state $|\psi(\tau_1, \tau_2)\rangle$ has the form of Eq. (7), with the JSA $\phi_0(\omega_1, \omega_2)$ replaced by the delayed JSA

$$\phi(\omega_1, \omega_2; \tau_1, \tau_2) = \phi_0(\omega_1, \omega_2)e^{-i\omega_1\tau_1 - i\omega_2\tau_2}. \tag{11}$$

Estimating shifts in the delay parameters is therefore equivalent to estimating shifts in the phase gradient of the postevolution JSA.

C. Precision bounds for a single unknown delay

We turn now to the specific QCRB applicable to two-photon timing measurements. First, we briefly review the problem of estimating the delay τ_1 when the delay τ_2 is known in advance, for which the QCRB has been derived previously in Ref. [8]. In Ref. [13] it was shown that the QFI for a transformation characterized by the single parameter g and the generator $\hat{G}$ is $\mathcal{Q}_g = 4\langle\hat{G}^2\rangle - 4\langle\hat{G}\rangle^2$. If the only unknown parameter is τ_1, generated by $\hat{\Omega}_1$ as in Eq. (9a), then the QFI for the problem is

$$\mathcal{Q}_{\tau_1} = 4\langle\hat{\Omega}_1^2\rangle_0 - 4\langle\hat{\Omega}_1\rangle_0^2 = 4\langle\Delta^2\hat{\Omega}_1\rangle_0 \equiv 4(\Delta\omega_1)^2, \tag{12}$$

where $\Delta\omega_1$ denotes the root mean square (rms) angular frequency bandwidth of the photon in mode 1. The single-parameter QCRB then limits the per-trial measurement precision to $\Delta\tau_1 \geqslant 1/2\Delta\omega_1$. In this case, the single-parameter QCRB is equivalent to the Heisenberg-like time-bandwidth inequality $\Delta\tau_1\Delta\omega_1 \geqslant \frac{1}{2}$. The use of a two-photon measurement may confer technical advantages in this situation, such as the phase insensitivity and dispersion cancellation properties of the HOM measurement, but no improvement in precision is possible relative to an optimal single-photon measurement.

D. Precision bounds for two unknown delays

We now consider the QCRB applicable to estimation in the presence of two unknown delays τ_1 and τ_2 or equivalently τ_- and τ_+. This general analysis is directly comparable to the particular case of HOM interferometry, discussed in Sec. III, in which the interferometer must estimate τ_- using a measurement insensitive to τ_+. We express the QCRB for the relative delay τ_- in terms of the bandwidths of the individual arms $\Delta\omega_{1,2}$ and the frequency correlations (quantified by the covariance C) between the two arms. Since this situation involves multiple unknown parameters, the QCRB must be

calculated through the use of the quantum Fisher information matrix. This matrix encodes not only the precision limits due to quantum-mechanical limitations on the measurement process, but also the manner in which additional unknown parameters of the probe state (here τ_+) may degrade the precision of estimates of a quantity of interest (here τ_-).

As in the case of the single-parameter quantum Fisher information, the quantum Fisher information matrix may be calculated in terms of generators of the individual parameters. As shown in Ref. [13], if $\hat{G}_i$ denotes the generator of parameter i, then $\mathcal{Q}_{ij} = 2\langle\{\hat{G}_i, \hat{G}_j\}\rangle_0 - 4\langle\hat{G}_i\rangle_0\langle\hat{G}_j\rangle_0$, where $\{\cdot, \cdot\}$ denotes the anticommutator. We evaluate these bounds for the problem of estimating τ_- and τ_+, which have generators $\hat{\Omega}_\pm$ defined following Eq. (10). The quantum Fisher information matrix elements are then

$$\mathcal{Q}_{++} = 4\langle\Delta^2\hat{\Omega}_+\rangle_0 = 4\Delta\omega_1^2 + 4\Delta\omega_2^2 + 8C, \tag{13a}$$

$$\mathcal{Q}_{--} = 4\langle\Delta^2\hat{\Omega}_-\rangle_0 = 4\Delta\omega_1^2 + 4\Delta\omega_2^2 - 8C, \tag{13b}$$

$$\mathcal{Q}_{+-} = \mathcal{Q}_{-+} = 4\langle\hat{\Omega}_+\hat{\Omega}_-\rangle_0 - 4\langle\hat{\Omega}_+\rangle_0\langle\hat{\Omega}_-\rangle_0$$
$$= 4\Delta\omega_1^2 - 4\Delta\omega_2^2. \tag{13c}$$

Here $\Delta\omega_1$ and $\Delta\omega_2$ continue to refer to the rms angular frequency bandwidths of the photons in modes 1 and 2 and we introduce the frequency covariance between the two modes

$$C = \langle\hat{\Omega}_1\hat{\Omega}_2\rangle_0 - \langle\hat{\Omega}_1\rangle_0\langle\hat{\Omega}_2\rangle_0. \tag{14}$$

Values of $C > 0$ describe photons with frequency correlations and $C < 0$ describes photons with frequency anticorrelations. The off-diagonal elements of the quantum Fisher information matrix $\mathcal{Q}_{+-} = \mathcal{Q}_{-+}$ vanish only when the two photons have equal bandwidths. It follows from our discussion of Eq. (6) that for probe states with $\Delta\omega_1 \neq \Delta\omega_2$, a lack of information about the mean delay τ_+ leads also to a decrease in the possible precision of estimates of τ_-.

A key result of this paper is the derivation of effective QFI for measurements of the relative delay τ_- and mean delay τ_+. Combining Eq. (13) with Eq. (6), we arrive at expressions for the effective QFIs in terms of the single-mode bandwidths and the two-photon frequency covariance

$$\mathcal{Q}_{\text{eff}}^{(+)} = 16\frac{\Delta\omega_1^2\Delta\omega_2^2 - C^2}{\Delta\omega_1^2 + \Delta\omega_2^2 - 2C}, \tag{15a}$$

$$\mathcal{Q}_{\text{eff}}^{(-)} = 16\frac{\Delta\omega_1^2\Delta\omega_2^2 - C^2}{\Delta\omega_1^2 + \Delta\omega_2^2 + 2C}. \tag{15b}$$

Together with Eq. (5), these expressions provide precision bounds for any measurement of these delays using a two-photon state of the form of Eq. (7), regardless of the specific JSA used. Taken alone, the bound obtained from Eq. (15b) limits the precision of measurements such as the HOM measurement that estimates the relative photon delay τ_- in the absence of prior information about τ_+.

Plots of Eqs. (15) are shown in Fig. 2, normalized to the product of the two-mode bandwidths $\Delta\omega_1$ and $\Delta\omega_2$. When the photons have equal bandwidths $\Delta\omega_1 = \Delta\omega_2$, maximal anticorrelations provide optimal precision in measurements of τ_-, at the expense of reduced precision for measurements of τ_+. If the photon bandwidths are not equal, measurements with nonmaximal frequency anticorrelations offer the opti-

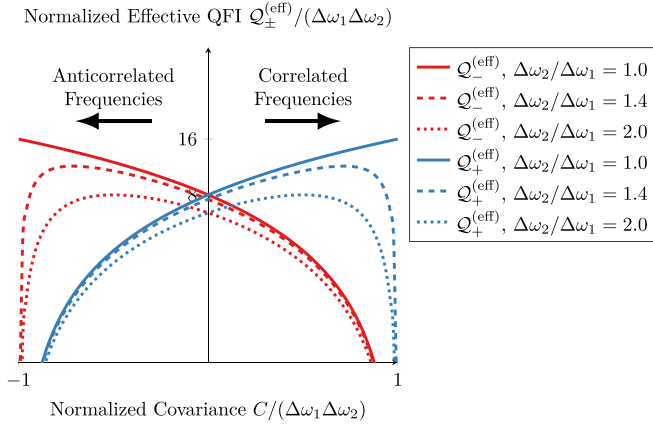Normalized Effective QFI $\mathcal{Q}_\pm^{(\text{eff})}/(\Delta\omega_1\Delta\omega_2)$

FIG. 2. Effective quantum Fisher information that determines the maximum possible precision of measurements of the relative delay τ_- (red, upper left curves) and the mean delay τ_+ (blue, upper right curves), displayed on a logarithmic scale. The case of equal photon bandwidths $\Delta\omega_1 = \Delta\omega_2$ shows maximum timing precision when the photons are maximally (anti)correlated. If the photons have different bandwidths, the optimal precision occurs when the frequency covariance is reduced from its maximum value. Note that the effective QFI shown here is normalized by the product of both photon bandwidths to emphasize the symmetry between $\mathcal{Q}_-^{(\text{eff})}$ and $\mathcal{Q}_+^{(\text{eff})}$. Later plots normalize the effective QFI to only one photon bandwidth.

mal precision. Likewise, when the probe photons have equal bandwidths, the optimal precision for measurements of τ_+ occurs when the photons are maximally correlated in frequency. When the photon bandwidths are not equal, nonmaximal frequency correlations give the best precision for measurements of τ_+. The optimal precision for measurements of $\tau_\pm$ occurs at a frequency covariance of $C_{\text{opt}} = \pm \min[(\Delta\omega_1)^2, (\Delta\omega_2)^2]$, for which the QCRBs for the two parameters are (after applying the Cauchy-Schwarz inequality $|C| \leqslant \Delta\omega_1\Delta\omega_2$) $\Delta\tau_\pm \geqslant \frac{1}{4\sqrt{n}} \max[1/\Delta\omega_1, 1/\Delta\omega_2]$. The smaller of the two-photon bandwidths ultimately sets the precision limits for estimation of either parameter. This behavior occurs only for the optimal covariance value C_{opt}, with measurements having worse precision at other values of C. Proper tuning of the two-photon frequency correlations becomes important whenever the photon bandwidths are not equal.

We now give strategies to attain optimal precision in a few specific scenarios. First, we consider estimation of τ_- when the mean delay τ_+ is not known. If the probe state must have strong frequency anticorrelations, as is the case for cw-pumped down-conversion sources of photon pairs, it is crucial to have photon bandwidths that are very nearly equal. On the left-hand side of Fig. 2 we see a rapid decline in precision of τ_- measurements when the photon bandwidths are not equal. In Fig. 3 we plot the QCRB for estimates of τ_- when one photon (the photon at ω_1, for concreteness) is restricted to a particular bandwidth $\Delta\omega_1$. The precision limits are normalized to the bandwidth of this photon. If the photon bandwidths are equal, we again see optimal precision for strongly anticorrelated states. These anticorrelated states are however highly sensitive to errors in the bandwidth ratio. If the second bandwidth may be tuned, then uncorrelated states with a large bandwidth ratio $\Delta\omega_2/\Delta\omega_1$ offer the same precision
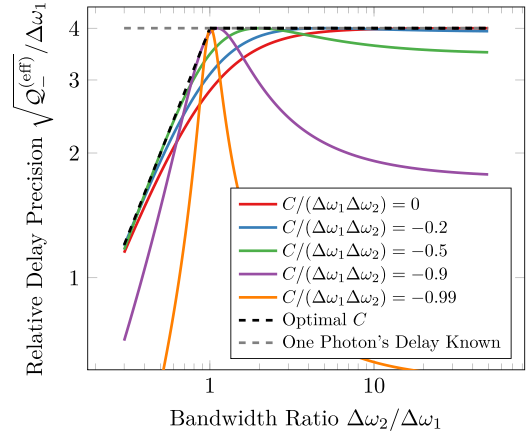

FIG. 3. Maximum precision for arbitrary measurements of the relative photon delay τ_-, equal to the inverse of the minimum relative delay that can be resolved and normalized to the bandwidth of one of the photons. Larger values of the delay precision correspond to more sensitive timing measurements. The vertical and horizontal scales of this plot are both logarithmic. The colored (lower) curves indicate the precision limits when the mean delay of the two photons is not known, for different values of the frequency covariance C defined in Eq. (14). Starting at the upper right corner of the figure and moving downward, the curves correspond to normalized covariances of 0, -0.2, -0.5, -0.9, and -0.99, respectively. The light dashed line along the top of the figure indicates the precision limit when the delay of one of the photons is known in advance; this limit is independent of C. The dark dashed line indicates the optimal delay precision for a given bandwidth ratio.

with less sensitivity to the exact values of the bandwidth, potentially allowing for an increase in precision if the bandwidth of one photon is not known in advance. In any situation, precision estimation of τ_- requires proper selection of both the bandwidth ratio and the frequency covariance of the state.

The upper dashed line in Fig. 3 is the bound obtained from the analysis of a single unknown delay in Ref. [8]. As the unknown parameter in this case is a single-photon property, it is independent of any shared properties of the photon pair, such as the frequency entanglement or the ratio of photon bandwidths. The bound on τ_- we derive describes estimation of a parameter shared between both photons (a relative time delay) and so the estimation precision for this delay has a strong dependence not only on the single-photon properties, but also on these properties of the photon pair.

We consider now to estimation of τ_- when the delay of the photon in mode $\hat{a}_2$ is known in advance. Comparing the effective QFI of Eq. (15b) to the single-parameter QFI of Eq. (12), we see that knowledge of one photon's delay allows estimation of the relative delay τ_- at the optimal precision regardless of the photon bandwidth and of the two-photon frequency covariance. We note that the factor of 4 difference between Eqs. (15b) and (12) is due to our definition of $\tau_- \equiv (\tau_1 - \tau_2)/2$. If τ_2 is fixed at a particular value, then a shift of $\delta\tau_1$ leads to $\delta\tau_- = \delta\tau_1/2$ so that $\Delta^2\tau_1 \sim \Delta^2\tau_-/4$ and the QCRB contains an additional factor of 4. In this case, estimation of τ_- is equivalent to estimation of τ_1 alone, so we return to the single-parameter single-particle estimation problem, for which two-photon properties play no role.
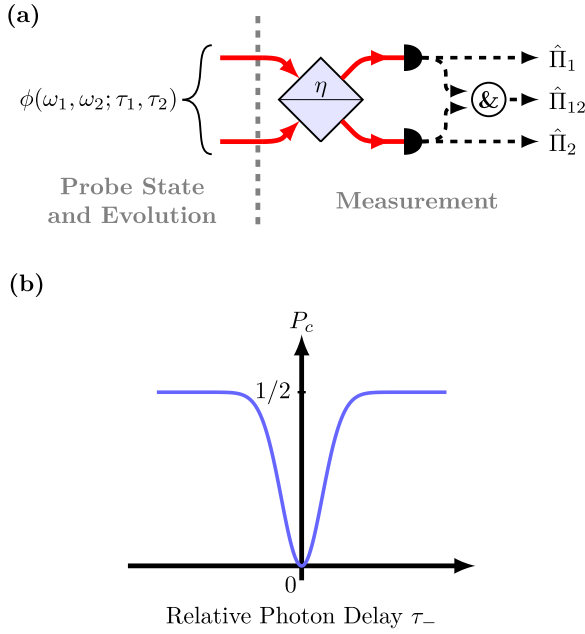
(a)

(b)

FIG. 4. (a) Hong-Ou-Mandel measurement scheme. A beam splitter of reflectivity η, typically with $\eta = 0.5$, interferes the two spatial modes. The output ports are monitored by single-photon detectors, and the number of single counts (projectors $\hat{\Pi}_1$ and $\hat{\Pi}_2$), as well as the number of coincident counts (projector $\hat{\Pi}_{12}$), are recorded. The proportion of probe states leading to a coincident detection is used to estimate the relative delay $\tau_- \equiv (\tau_1 - \tau_2)/2$. (b) Hong-Ou-Mandel interference, which appears as a dip in the probability of a coincidence detection as the relative delay τ_- approaches zero. The reduction in the coincidence probability is due to both photons leaving from the same output port of the beam splitter.

III. HONG-OU-MANDEL MEASUREMENT PRECISION

This section examines the precision limits specific to the Hong-Ou-Mandel timing measurement. In Sec. III A we find expressions for the coincidence probability given an arbitrary two-photon JSA and use them to derive the classical Fisher information for estimation of τ_-. In Sec. III B we examine the specific case of a probe state with a JSA that is Gaussian in the two frequencies ω_1 and ω_2. We then compare this to the fundamental bounds given in Sec. II.

The HOM measurement (Fig. 4) involves interference of the two spatial modes at a beam splitter, followed by detection by a single-photon detector placed at each output port. The rate of coincidence detections between the two detectors is then recorded. In practice, many photon pairs arrive in succession at the detectors, so spurious coincidence events consisting of one photon from each of two-photon pairs may occur. This is avoided by the use of time-resolving detectors and gated coincidence counting, so detections due to different photon pairs may be distinguished. The time resolution used for this purpose is typically insufficient to measure the relative delay τ_- of the photon pairs at the precision required. We therefore neglect any time resolution of the detectors themselves and focus instead on the timing resolution inherent to the HOM measurement itself.

A. Detection probabilities and timing precision

We calculate here the detection probabilities for single and coincidence counts. The HOM measurement consists of a beam splitter with intensity reflectance η and detection of the resulting state by a pair of single-photon detectors. The initial state (7) is described by the JSA $\phi_0(\omega_1, \omega_2)$. After evolution, the JSA now takes the form $\phi(\omega_1, \omega_2; \tau_1, \tau_2)$, defined in Eq. (11). We model the beam-splitter action as

$$\hat{a}_1^\dagger(\omega) \rightarrow \sqrt{\eta}\hat{a}_1^\dagger(\omega) + i\sqrt{1-\eta}\hat{a}_2^\dagger(\omega), \qquad (16a)$$

$$\hat{a}_2^\dagger(\omega) \rightarrow i\sqrt{1-\eta}\hat{a}_1^\dagger(\omega) + \sqrt{\eta}\hat{a}_2^\dagger(\omega), \qquad (16b)$$

which neglect any frequency dependence on η. A value of $\eta = 0.5$ is commonly used to maximize the HOM interference effect. After the beam splitter, the photon pair has the state

$$\begin{aligned}|\psi(\tau_1, \tau_2)\rangle = {} & i\sqrt{\eta(1-\eta)}\,|\psi_{11}(\tau_1, \tau_2)\rangle \\ & + i\sqrt{\eta(1-\eta)}\,|\psi_{22}(\tau_1, \tau_2)\rangle + |\psi_{12}(\tau_1, \tau_2)\rangle,\end{aligned}$$
$$(17)$$

with $|\psi_{ii}(\tau_1, \tau_2)\rangle$ and $|\psi_{12}(\tau_1, \tau_2)\rangle$ describing pairs of photons at the same output port and at different output ports, respectively. These are in turn expressed in terms of the JSA of the delayed two-photon state by

$$|\psi_{ii}(\tau_1, \tau_2)\rangle = \iint d\omega_1 d\omega_2 \phi(\omega_1, \omega_2; \tau_1, \tau_2)\hat{a}_i^\dagger(\omega_1)\hat{a}_i^\dagger(\omega_2)|0\rangle \quad (i = 1, 2), \qquad (18a)$$

$$|\psi_{12}(\tau_1, \tau_2)\rangle = \iint d\omega_1 d\omega_2 [\eta\phi(\omega_1, \omega_2; \tau_1, \tau_2) - (1-\eta)\phi(\omega_2, \omega_1; \tau_1, \tau_2)]\hat{a}_1^\dagger(\omega_1)\hat{a}_2^\dagger(\omega_2)|0\rangle. \qquad (18b)$$

The detection probabilities are obtained from the projectors $\hat{\Pi}_i$, describing detection at a single output, and from the projector

$$\hat{\Pi}_{12} = \iint d\omega_1 d\omega_2 \hat{a}_1^\dagger(\omega_1)\hat{a}_2^\dagger(\omega_2)|0\rangle\langle 0|\hat{a}_1(\omega_1)\hat{a}_2(\omega_2), \qquad (19)$$

describing a coincidence event. Our definition of $\hat{\Pi}_{12}$ implicitly ignores any time resolution of the detectors, so the probability amplitudes for detection at different frequencies may be incoherently summed. The opposite limit, of infinitely fast detectors, involves additional terms describing single- and two-photon interference at different frequencies [16]. In Appendix B we examine a more realistic model which includes a finite-time resolution and show that the results given

for a non-time-resolving measurement are recovered when the timescale of the detector resolution is much longer than the duration of the input photons. In Appendix B it is also shown that the probability of detection at a single detector does not depend on τ_1 or τ_2 in the limit of poor detector time resolution. These events therefore do not contribute a useful signal for parameter estimation. From Eqs. (17)–(19) we find that the probability P_c for a given photon pair to lead to a coincidence count is

$$
\begin{aligned}
P_c &\equiv \langle \psi(\tau_1, \tau_2) | \hat{\Pi}_{12} | \psi(\tau_1, \tau_2) \rangle = \iint d\omega_1 d\omega_2 |\eta\phi \\
&\quad \times (\omega_1, \omega_2; \tau_1, \tau_2) - (1-\eta)\phi(\omega_2, \omega_1; \tau_1, \tau_2)|^2 \\
&= \eta^2 + (1-\eta)^2 - 2\eta(1-\eta) \text{Re} \iint d\omega_1 d\omega_2 \phi_0 \\
&\quad \times (\omega_1, \omega_2)\phi_0^*(\omega_2, \omega_1) e^{-2i(\omega_1 - \omega_2)\tau_-},
\end{aligned}
\tag{20}
$$

where the final expression is in terms of the JSA of the probe state before any delays are implemented.

The coincidence signal depends only on the combination $\tau_- = (\tau_1 - \tau_2)/2$, so the mean delay τ_+ cannot be estimated using the HOM measurement. Since only the final term depends on the delay parameters, it is advantageous to choose the value of η leading to the largest τ_--dependent signal while minimizing the τ_--independent contributions to the measured signal, which together maximize the classical Fisher information [Eq. (2)]. For any two-photon state, the conventional choice of a 50:50 beam splitter ($\eta = 0.5$) satisfies both conditions and leads to the optimal signal for timing measurements. We exclusively consider $\eta = 0.5$ for the remainder of our analysis. The coincidence probability then becomes

$$
\begin{aligned}
P_c &= \frac{1}{2} - \frac{1}{2} \text{Re} \iint d\omega_1 d\omega_2 \phi_0(\omega_1, \omega_2)\phi_0^*(\omega_2, \omega_1) \\
&\quad \times e^{-2i(\omega_1 - \omega_2)\tau_-}.
\end{aligned}
\tag{21}
$$

If the JSA of the probe state is symmetric between the two photons, $\phi(\omega_1, \omega_2) = \phi(\omega_2, \omega_1)$, the coincidence probability decreases to zero at $\tau_- = 0$. More general probe states will not show a null at zero relative delay, but the decrease in coincidence events may still be used to estimate the relative delay τ_-. The visibility of interference at $\tau_- = 0$ is determined by the overlap integral between the input JSA and a copy of the input JSA reflected over the line $\omega_1 = \omega_2$,

$$
\lim_{\tau_- \to 0} V = \text{Re} \iint d\omega_1 d\omega_2 \phi(\omega_1, \omega_2)\phi^*(\omega_2, \omega_1).
\tag{22}
$$

As noted in Sec. II A, the timing precision attainable with a HOM interferometer is $(\Delta\tau_-)_{\min} = 1/\sqrt{n\mathcal{F}}$, with the CFI obtained from P_c by $\mathcal{F} = (\partial P_c / \partial \tau_-)^2 / P_c$. For pairs with near-zero relative delay, the CFI takes the simplified form

$$
\lim_{\tau_- \to 0} \mathcal{F} = 4 \iint d\omega_1 d\omega_2 (\omega_1 - \omega_2)^2 \phi_0(\omega_1, \omega_2)\phi_0^*(\omega_2, \omega_1).
\tag{23}
$$

Maximizing the CFI in this case requires the use of anticorrelated frequencies, for which $|\omega_1 - \omega_2|$ is large, and also requires that $\phi_0(\omega_1, \omega_2)\phi_0^*(\omega_2, \omega_1)$ remain nonzero over a large range of frequencies. From Eq. (22) the condition that $\phi^*(\omega_2, \omega_1)\phi(\omega_1, \omega_2)$ be large is simply a requirement for high interference visibility. To gain further insight into relation

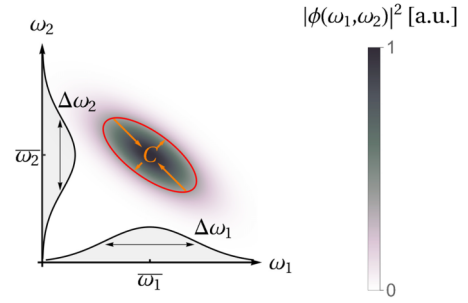Joint Spectral Intensity of Gaussian Probe State

FIG. 5. Two-photon probe state, with Gaussian joint spectral amplitude. The color bar indicates the magnitude of the joint spectral intensity (equal to the squared magnitude of the joint spectral amplitude) in arbitrary units. The marginal distributions are centered at frequencies $\overline{\omega}_1$ and $\overline{\omega}_2$ and have bandwidths $\Delta\omega_1$ and $\Delta\omega_2$, respectively. The covariance parameter C describes the strength of any frequency correlations ($C > 0$) or anticorrelations ($C < 0$) of the two photons. The covariance ellipse, defined as the contour where the joint spectral intensity takes the value $|\phi(\omega_1, \omega_2)|^2 = e^{-1/2}$, is outlined in red.

between $\mathcal{F}$ and the optical properties of the input state, such as the photon bandwidths and frequency entanglement, we focus now on the behavior of $\mathcal{F}$ for a particularly simple family of input states.

B. Probe states with Gaussian JSAs

A large class of JSAs encountered in practice, consisting of a central lobe at mean frequencies $\overline{\omega}_1$ and $\overline{\omega}_2$, may be approximated by a Gaussian distribution. This allows for analytical expressions of the coincidence probability and CFI to be obtained in terms of the mean frequencies, the photon bandwidths $\Delta\omega_1$ and $\Delta\omega_2$, and the frequency covariance C. Consider the special case of a probe state with a JSA of the form

$$
\phi_0(\omega_1, \omega_2) = N \exp[-\tfrac{1}{4}(\vec{\omega} - \vec{\Omega})^T \mathbf{\Sigma}^{-1}(\vec{\omega} - \vec{\Omega})],
\tag{24}
$$

where $\vec{\omega} \equiv (\omega_1, \omega_2)^T$. Here $\vec{\Omega} = (\overline{\omega}_1, \overline{\omega}_2)^T$ is a vector composed of the mean photon frequencies, $\mathbf{\Sigma}$ is a matrix describing the photon bandwidths and correlations in the spectral amplitudes of the photons, and N is a normalization constant. The matrix $\mathbf{\Sigma}$ has elements

$$
\mathbf{\Sigma} = \begin{pmatrix} (\Delta\omega_1)^2 & C \\ C & (\Delta\omega_2)^2 \end{pmatrix}.
\tag{25}
$$

These parameters are depicted in Fig. 5. The normalization constant $N = (2\pi\sqrt{\det \mathbf{\Sigma}})^{-1/2}$ is determined by the normalization condition (8).

For the Gaussian JSA of Eq. (24), the coincidence probability (20) has a Gaussian-shaped dip

$$
P_c = \tfrac{1}{2}[1 - V \exp(-\tau_-^2 / 2T^2)],
\tag{26}
$$

with width

$$
T = \frac{1}{4}\sqrt{\frac{\Delta\omega_1^2 + \Delta\omega_2^2 + 2C}{\Delta\omega_1^2 \Delta\omega_2^2 - C^2}}.
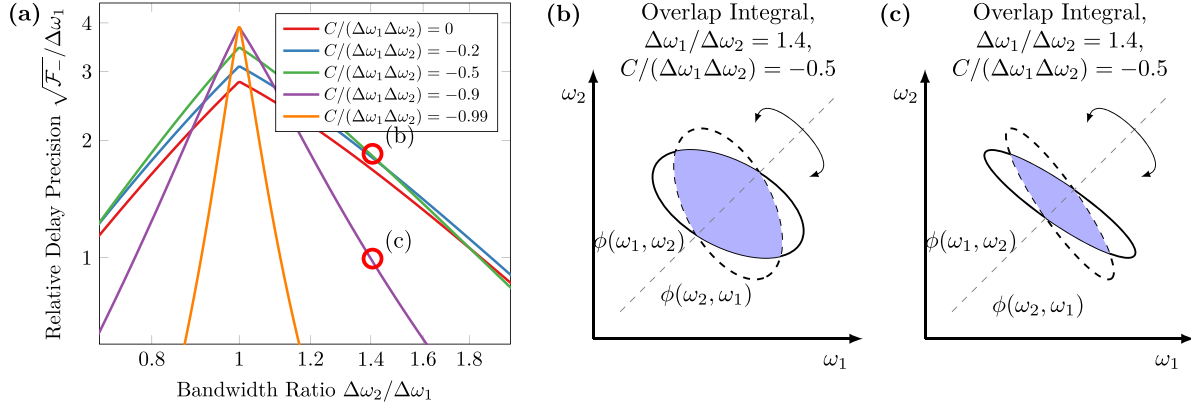\tag{27}
$$

FIG. 6. (a) Maximum precision for HOM measurements of the relative photon delay τ_-, equal to the inverse of the minimum relative delay that can be resolved by the HOM measurement and normalized to the bandwidth of one of the photons. Larger values of the delay precision correspond to more sensitive timing measurements. Note that the horizontal axis has a linear scale, different from Fig. 3. Different curves correspond to the precision limits of two-photon states with different values of the normalized frequency covariance $C/\Delta\omega_1\Delta\omega_2$. Starting at the bottom of the line $\Delta\omega_2/\Delta\omega_1 = 1$ and moving upward, the curves correspond to normalized covariances of 0, -0.2, -0.5, -0.9, and -0.99, respectively. (b) and (c) Depictions of the overlap integrals between the JSA $\phi(\omega_1, \omega_2)$ and the reflected function $\phi(\omega_2, \omega_1)$ in terms of the covariance ellipse of the JSA, defined by the equation $|\phi(\omega_1, \omega_2)|^2 = e^{-1/2}$. This overlap integral determines the interference visibility of the HOM dip. For states with unequal photon bandwidths, anticorrelated distributions are no longer exactly aligned with the antidiagonal of the diagram and correlated distributions are not aligned with the diagonal, leading to a reduction in interference visibility. (b) States with weak frequency correlations have broad JSAs whose interference pattern is less sensitive to a mismatch in the photon bandwidths; (c) states with strong correlations have narrower JSAs, so the interference visibility is more sensitive to any bandwidth mismatch. The net result is that, for mismatched photon bandwidths, strongly correlated states have a reduced precision relative to less correlated states.

Here

$$V = 2\sqrt{\frac{(\Delta\omega_1)^2(\Delta\omega_2)^2 - C^2}{[(\Delta\omega_1)^2 + (\Delta\omega_2)^2]^2 - 4C^2}}$$

$$\times \exp\left(-\frac{(\overline{\omega}_1 - \overline{\omega}_2)^2}{2(\Delta\omega_1^2 + \Delta\omega_2^2 - 2C)}\right) \qquad (28)$$

is the HOM interference visibility. The CFI takes the form

$$\mathcal{F} = \frac{1}{T^2}\left(\frac{\tau_-^2}{2T^2}\frac{(Ve^{-\tau_-^2/2T^2})^2}{1 - Ve^{-\tau_-^2/2T^2}}\right). \qquad (29)$$

A similar expression was derived in Ref. [7] for the case of a Gaussian HOM dip with equal photon bandwidths $\Delta\omega_1 = \Delta\omega_2 = \Delta\omega$ and maximal frequency anticorrelations, for which $T \to 1/4\Delta\omega$. Our result generalizes this to the case of more general states with Gaussian JSAs of unequal bandwidths, unequal central wavelengths, and arbitrary amounts of correlation.

For the type of nondegenerate states considered in our model (those states with Gaussian JSAs), photons possessing different center wavelengths offer much poorer precision than similar photon pairs with the same bandwidths and correlations but degenerate center wavelengths. This is due to the exponential loss of visibility with increasingly nondegenerate pairs. This result contrasts with the nondegenerate pairs considered in previous analysis of the HOM interferometer [6,8] in which each spatial mode may contain a photon at either center wavelength. This latter type of state is still useful for enhanced timing metrology due to spectral indistinguishability between the two modes, in contrast with our result

showing a rapid decline of the CFI when degenerate pairs are used.

The effective QFI for this Gaussian JSA, given by Eq. (15b), is $\mathcal{Q}_{\text{eff}}^{(-)} = 1/T^2$. The HOM measurement is an optimal measurement (saturates the QCRB) only when the factor of Eq. (29) in large parentheses is unity, which occurs when both $\tau_- \to 0$ and $V \to 1$. From the expression (28) for the HOM visibility, this requires that the photons have identical properties $\overline{\omega}_1 = \overline{\omega}_2$ and $\Delta\omega_1 = \Delta\omega_2$. Though the HOM measurement saturates the QCRB at any value of the covariance C, the use of anticorrelated states still offers enhanced precision by reducing the HOM width T, given by Eq. (27), which increases both the effective QFI and the CFI for the parameter τ_-.

We consider now the situation in which one photon's bandwidth is restricted to a particular value and compare the performance of the HOM measurement to the ultimate precision bounds given in Sec. II. A plot of the CCRB for estimation of τ_- is shown in Fig. 6(a), which may be compared directly to the quantum bound of Fig. 3, noting the change of scale on the horizontal axis. Since the CCRB given in Eq. (29) depends on the value of τ_- about which shifts in the delay are measured, the precision bounds shown in Fig. 6 assume a value of τ_- that maximizes the timing precision of the measurement. For perfect interference visibility, this corresponds to the assumption of a properly zeroed HOM interferometer, with delays chosen to give $\tau_- = 0$ before measurements of any shift in τ_-. For imperfect visibility, the HOM interferometer has maximum visibility when the initial delay τ_- is slightly offset from zero, as was first noted in Ref. [7].

Both the QCRB and the CCRB show that anticorrelated states are most sensitive to estimation of τ_- when photon bandwidths are equal and that highly anticorrelated states

lose precision more quickly than uncorrelated states when the photon bandwidths become increasingly unbalanced. The HOM measurement is much more sensitive to changes in the bandwidth ratio than is required by the quantum bound, however, and the use of HOM interference using uncorrelated states with a large ratio of photon bandwidths does not yield high timing precision as was found for the QCRB.

For the arbitrary timing measurements considered in Sec. II, the exact physical reasons leading to the behavior of Fig. 3 are not apparent and would depend on the measurement in question. Focusing on the specific case of a HOM measurement provides some insight into the increase in precision with weaker anticorrelations when the photon bandwidths are not equal. In this case, the CFI at zero relative delay [Eq. (29)] involves a factor depending on the relative frequency $(\omega_1 - \omega_2)^2$ of the photons and a factor describing the overlap of the JSA $\phi(\omega_1, \omega_2)$ with a reflected JSA $\phi(\omega_2, \omega_1)$. The first factor is maximized when the JSA contains strong anticorrelations so that $|\omega_1 - \omega_2|$ is large for much of the state. The second factor is related to the interference visibility, which takes the form of Eq. (22). We see that increasing the CFI requires strong anticorrelations and a high interference visibility.

Focusing exclusively on Gaussian JSAs, we see from Figs. 6(b) and 6(c) that states with unequal bandwidths and frequency anticorrelations have a main extent that is not aligned with the antidiagonal of the ω_1-ω_2 space, but is instead rotated away from this antidiagonal, with an angle that increases with the ratio $\Delta\omega_1/\Delta\omega_2$ of the bandwidths. This rotation leads to a decreasing overlap between $\phi(\omega_1, \omega_2)$ and $\phi(\omega_2, \omega_1)$ and to a resulting loss of interference visibility. States with strong frequency anticorrelations have narrower JSAs than those states with weaker anticorrelations and lead to a decreased visibility relative to less correlated states as a result. When the photon bandwidths are not equal, then anticorrelated states which maximize $|\omega_1 - \omega_2|$ are hampered by a low interference visibility and offer less precise timing measurements than uncorrelated states which have a visibility less sensitive to the relative sizes of the photon bandwidths.

When the photon bandwidths are identical, frequency anticorrelated pairs provide high resolution. When the photons have unequal bandwidths, maximizing the resolution involves a tradeoff between the competing requirements for high visibility and strong anticorrelations in frequency.

IV. CONCLUSION

To summarize, we have examined theoretically the precision bounds of HOM interferometry in the important case where one photon has a smaller bandwidth than the other. Using the classical Fisher information for this measurement [Eq. (29)], we found that highly anticorrelated light is undesirable and instead the amount of frequency correlations must be tuned to a value determined by both of the photon bandwidths in order to obtain maximum precision. By examining the fundamental precision limits imposed on the measurement by quantum mechanics [Eq. (6)], we found that this behavior is not specific to the HOM interferometer and that similar limitations apply to any measurement of the relative time delay τ_- between a pair of photons that is insensitive to their mean delay τ_+. A different feature of our analysis is the fact that

the CFI for HOM measurements is bounded above both by the QFI found for a single unknown delay and by the effective QFI for measurements of τ_- in the presence of an unknown τ_+. This is due to the HOM measurement statistics being intrinsically insensitive to τ_+ so that the CFI for measurements of τ_- has the same value regardless of whether τ_+ is known in advance. Compared to the previous analysis in Refs. [7,8], our analysis also demonstrated the relation of the timing precision to the two-photon properties of frequency entanglement and bandwidth mismatch.

The fundamental bounds we derived are not specific to the standard HOM measurement scheme and apply to many modified measurements as well, such as the use of number-, time-, or frequency-resolving detectors [18,26], as well as the use of more complicated estimators that rely on more than just the coincidence probability. Nevertheless, as the standard HOM measurement we considered does not saturate these fundamental bounds for most probe states, the possibility of improving the HOM scheme beyond the precision of current techniques is compelling. Relevant to our analysis, we found that uncorrelated probe states with highly mismatched bandwidths may be used to perform timing measurements at the level of current precision HOM measurements without a strict requirement for equal bandwidths, which would be highly advantageous in circumstances involving transmission through an absorbing medium, where the final bandwidth of one photon is not under experimental control. Whether a measurement exists that can reach this precision while also keeping the many salutary properties of the HOM measurement is an open question.

We believe that insight into the fundamental limitations of precision measurements will benefit the development of future metrological schemes both by identifying the key features necessary to increase precision and by identifying those features that cannot be improved beyond current limitations. Our analysis highlighted the essential features of HOM interferometry that must be considered when one or more photon bandwidths are constrained. By carefully tailoring the spectral properties of photon pairs, the techniques of precision HOM interferometry can reach beyond the laboratory in the continuing effort for increasingly precise measurements.

APPENDIX A: SUMMARY OF RESULTS

In this Appendix we briefly summarize the main mathematical results of our analysis. In all equations, $\Delta\omega_1$ and $\Delta\omega_2$ refer to the rms angular frequency bandwidths of photons 1 and 2 and C refers to the frequency covariance shared by the two photons.

1. Precision bounds of the HOM measurement

The HOM measurement is defined by the use of the measurement in Fig. 4(a) in the final stage of Fig. 1. This measurement may obtain a precision for estimates of the relative photon delay τ_- limited to $\Delta^2\tau_- \geqslant 1/n\mathcal{F}_{\tau_-}$ when the measurement is repeated n times, where $\mathcal{F}_{\tau_-}$ is the CFI.

If the JSA of the input photon pair has the form of a real two-dimensional Gaussian, then $\mathcal{F}_{\tau_-}$ has the form

$$\mathcal{F}_{\tau_-} = \frac{1}{T^2}\left(\frac{\tau_-^2}{2T^2}\frac{\left(Ve^{-\tau_-^2/2T^2}\right)^2}{1 - Ve^{-\tau_-^2/2T^2}}\right), \qquad (A1)$$

where the width T of the HOM dip is

$$T = \frac{1}{4}\sqrt{\frac{\Delta\omega_1^2 + \Delta\omega_2^2 + 2C}{\Delta\omega_1^2\Delta\omega_2^2 - C^2}} \qquad (A2)$$

and the HOM visibility is

$$V = 2\sqrt{\frac{(\Delta\omega_1)^2(\Delta\omega_2)^2 - C^2}{\left((\Delta\omega_1)^2 + (\Delta\omega_2)^2\right)^2 - 4C^2}}$$

$$\times \exp\left(-\frac{(\overline{\omega}_1 - \overline{\omega}_2)^2}{2\left(\Delta\omega_1^2 + \Delta\omega_2^2 - 2C\right)}\right). \qquad (A3)$$

Here $\overline{\omega}_1$ and $\overline{\omega}_2$ are the mean angular frequencies of the two photons.

2. Precision limits for generalized measurements with a single unknown delay

The generalized measurement we consider has the form of Fig. 1, with any set of projectors allowed as the measurement. The timing precision possible with this form of measurement is bounded by

$$\Delta^2\tau_i \geqslant 1/4n(\Delta\omega_i)^2 \qquad (A4)$$

when the measurement is repeated n times, where ω_i is the angular frequency of the photon undergoing the delay τ_i. The precision bounds of the relative delay $\tau_- = (\tau_1 - \tau_2)/2$ and of the mean delay $\tau_+ = (\tau_1 + \tau_2)/2$ are $\Delta^2\tau_\pm \geqslant 1/16n(\Delta\omega_i)^2$.

3. Precision limits for generalized measurements with two unknown delays

If neither delay τ_1 or τ_2 is known in advance, the precision of the generalized measurement of Fig. 1 for estimates of $\tau_\pm = (\tau_1 \pm \tau_2)/2$ is in this case bounded by $\Delta^2\tau_\pm \geqslant 1/n\mathcal{Q}_{\text{eff}}^{(\pm)}$, where the effective QFI $\mathcal{Q}_{\text{eff}}^{(\pm)}$ is

$$\mathcal{Q}_{\text{eff}}^{(\pm)} = 16\frac{\Delta\omega_1^2\Delta\omega_2^2 - C^2}{(\Delta\omega_1)^2 + (\Delta\omega_2)^2 \mp 2C}. \qquad (A5)$$

As discussed in Sec. II, these are also the bounds that apply to measurements of $\tau_\pm$ that are insensitive to the other delay $\tau_\mp$.

APPENDIX B: MODEL OF TIME-RESOLVED HOM INTERFEROMETRY

This Appendix examines the effect of time-resolved photon detection as it pertains to estimation of the delays τ_- and τ_+. We show how the results of Sec. III for a HOM measurement with no time resolution emerge from a model that includes time resolution. A more detailed analysis of the effect of time resolution for estimation of a single unknown delay is available in Ref. [18]. We begin with a model of time-, frequency-, and number-resolving measurement and from that obtain a model of detection that is time resolving, but not frequency or number resolving. We then apply this detector model to find the probability distribution describing the measurement outcomes, which is related to the multiparameter CCRB in a manner similar to the single-parameter CCRB discussed in Sec. II A.

A measurement scheme is determined by its positive-operator-valued measure (POVM) $\{\hat{\Pi}_i\}$, with each operator $\hat{\Pi}_i$ describing a measurement outcome i. Our model assumes a detection process that is described by projectors onto the pure states

$$|\zeta_{T_D\omega_D}\rangle_i = \int d\omega\, \zeta_{T_D\omega_D}(\omega)\hat{a}_i^\dagger(\omega)|0\rangle, \; |\zeta_{T_D\omega_D}\zeta_{T_D'\omega_D'}\rangle_{ij}$$

$$= \iint d\omega\, d\omega'\zeta_{T_D\omega_D}(\omega)\zeta_{T_D'\omega_D'}(\omega')\hat{a}_i^\dagger(\omega)\hat{a}_j^\dagger(\omega')|0\rangle, \tag{B1}$$

which describe a single photon at detector $i = 1, 2$ and a pair of photons at each of the detectors $i, j = 1, 2$, respectively. In the latter case, the labels i and j may be equal, describing a measurement of two photons at the same detector; in this case, we require that the detection times are labeled with $T_D' > T_D$. The labels $\zeta_{T_D\omega_D}$ refer to a time-frequency bin centered at time T_D and frequency ω_D so that T_D refers to the time bin of the detected photon and ω_D refers to its frequency bin. The POVM describing the measurement then consists of all projectors $\hat{\Pi}_{i,T_D\omega_D} \propto |\zeta_{T_D\omega_D}\rangle_{i\,i}\langle\zeta_{T_D\omega_D}|$ and $\hat{\Pi}_{i,T_D\omega_D;j,T_D'\omega_D'} \propto |\zeta_{T_D\omega_D}\zeta_{T_D'\omega_D'}\rangle_{ij\,ij}\langle\zeta_{T_D\omega_D}\zeta_{T_D'\omega_D'}|$, where the proportionality constants are chosen so that the POVM elements sum to the identity. The detection probabilities for a detector that is only time resolving, and not number or frequency resolving, may be obtained by summing over the probabilities of all measurement outcomes with the same time bin.

In performing this sum, we also add the probabilities $\langle\hat{\Pi}_{i,T_D\omega_D;i,T_D'\omega_D'}\rangle$ of measuring two photons at port i to the probability $\langle\hat{\Pi}_{i,T_D\omega_D}\rangle$ of measuring only one photon at i, as a detector insensitive to photon number will not distinguish these events. In doing so, the time bin of the second photon, T_D', is discarded, as the second photon arrives during the dead time of the detector is ignored. This final time-resolved detection is described by four probabilities: the probability p_0 of observing no click at either detector, the probability $p_i(T_D)$ ($i = 1, 2$) of observing a click at detector i within time bin T_D, and the probabilities $p_{12}(T_D, T_D')$ ($i = 1, 2$) of observing a click at detector one in time bin T_D and a click at detector two in time bin T_D'. For a two-photon input state $|\psi\rangle$, these

probabilities have the form

$$
p_i(T_D) = \int d\omega_D \langle \psi | \hat{\Pi}_{i,T_D\omega_D} | \psi \rangle
$$
$$
+ \int dT_D' \iint d\omega_D d\omega_D' \langle \psi | \hat{\Pi}_{i,T_D\omega_D;i,T_D'\omega_D'} | \psi \rangle ,
$$
$$
p_{12}(T_D, T_D') = \iint d\omega_D d\omega_D' \langle \psi | \hat{\Pi}_{i,T_D\omega_D;i,T_D'\omega_D'} | \psi \rangle ,
$$
$$
p_0 = 1 - \int dT_D p_1(T_D) - \int dT_D p_2(T_D)
$$
$$
- \iint dT_D dT_D' p_{12}(T_D, T_D'). \tag{B2}
$$

To calculate these probabilities, a specific form of the time-frequency bins $\zeta_{T_D,\omega_D}(\omega)$ must be specified.

We focus on the case of Gaussian time-frequency bins, for which

$$
\zeta_{T_D,\omega_D}(\omega) = \left(\frac{2\tau^2}{\pi} \right)^{1/4} e^{-\tau^2(\omega-\omega_D)^2} e^{i\omega T_D}. \tag{B3}
$$

The detection probabilities of a time-resolved detector are most easily expressed in terms of the joint temporal amplitude of the input state $\tilde{\phi}_0$, which is related to the JSA ϕ_0 by

$$
\tilde{\phi}_0(t, t') = \frac{1}{2\pi} \iint d\omega\, d\omega'\, \phi_0(\omega, \omega') e^{-i\omega t - i\omega' t'}. \tag{B4}
$$

The time-resolved detection probabilities are found to be

$$
p_0 = (1-\theta)^2,
$$
$$
p_1(T_D) = \frac{\theta(1-\theta)(1-\eta)}{\sqrt{2\pi\tau^2}} \iint dt\, dt' |\tilde{\phi}_0(t', t)|^2 e^{-[t+T_D-(\tau_+-\tau_-)]^2/2\tau^2} + \frac{\theta(1-\theta)\eta}{\sqrt{2\pi\tau^2}} \iint dt\, dt' |\tilde{\phi}_0(t, t')|^2 e^{-[t+T_D-(\tau_++\tau_-)]^2/2\tau^2}
$$
$$
+ \frac{2\eta(1-\eta)\theta^2}{\sqrt{2\pi\tau^2}} \iint dt\, dt' |\tilde{\phi}_0(t+\tau_-, t'-\tau_-) + \tilde{\phi}_0(t'+\tau_-, t-\tau_-)|^2 e^{-(t+T_D-\tau_+)^2/2\tau^2},
$$
$$
p_2(T_D) = \frac{\theta(1-\theta)\eta}{\sqrt{2\pi\tau^2}} \iint dt\, dt' |\tilde{\phi}_0(t', t)|^2 e^{-[t+T_D-(\tau_+-\tau_-)]^2/2\tau^2} + \frac{\theta(1-\theta)(1-\eta)}{\sqrt{2\pi\tau^2}} \iint dt\, dt' |\tilde{\phi}_0(t, t')|^2 e^{-[t+T_D-(\tau_++\tau_-)]^2/2\tau^2}
$$
$$
+ \frac{2\eta(1-\eta)\theta^2}{\sqrt{2\pi\tau^2}} \iint dt\, dt' |\tilde{\phi}_0(t+\tau_-, t'-\tau_-) + \tilde{\phi}_0(t'+\tau_-, t-\tau_-)|^2 e^{-(t+T_D-\tau_+)^2/2\tau^2},
$$
$$
p_{12}(T_D, T_D') = \frac{\theta^2}{2\pi\tau^2} \iint dt\, dt' |\eta\tilde{\phi}_0^*(t+\tau_-, t'-\tau_-) - (1-\eta)\tilde{\phi}_0^*(t'+\tau_-, t-\tau_-)|^2 e^{-(t+T_D-\tau_+)^2/(2\tau^2)-(t'+T_D'-\tau_+)^2/(2\tau^2)}, \tag{B5}
$$

where θ is the efficiency of each detector and other variables have the same meaning as in the main text. In all four expressions, the mean delay τ_+ serves only to determine the time bin of the detected photons. The difference delay τ_-, however, affects the two-photon interference pattern seen in

p_{12}. If the duration of the input state $\tilde{\phi}_0$ is much shorter than the time resolution τ of the detector, then the exponentials vary slowly over the extent of the integral so that we obtain the approximate probabilities

$$
p_0 = (1-\theta)^2,
$$
$$
p_1(T_D) = \frac{\theta(1-\theta)}{\sqrt{2\pi\tau^2}} [(1-\eta)e^{-[T_D-(\tau_+-\tau_-)]^2/2\tau^2} + \eta e^{-[T_D-(\tau_++\tau_-)]^2/2\tau^2}] \iint dt\, dt' |\tilde{\phi}_0(t, t')|^2
$$
$$
+ \frac{2\eta(1-\eta)\theta^2}{\sqrt{2\pi\tau^2}} e^{-(T_D-\tau_+)^2/2\tau^2} \iint dt\, dt' |\tilde{\phi}_0(t+\tau_-, t'-\tau_-) + \tilde{\phi}_0(t'+\tau_-, t-\tau_-)|^2,
$$
$$
p_2(T_D) = \frac{\theta(1-\theta)}{\sqrt{2\pi\tau^2}} [\eta e^{-[T_D-(\tau_+-\tau_-)]^2/2\tau^2} + (1-\eta)e^{-[T_D-(\tau_++\tau_-)]^2/2\tau^2}] \iint dt\, dt' |\tilde{\phi}_0(t, t')|^2
$$
$$
+ \frac{2\eta(1-\eta)\theta^2}{\sqrt{2\pi\tau^2}} e^{-(T_D-\tau_+)^2/2\tau^2} \iint dt\, dt' |\tilde{\phi}_0(t+\tau_-, t'-\tau_-) + \tilde{\phi}_0(t'+\tau_-, t-\tau_-)|^2,
$$
$$
p_{12}(T_D, T_D') = \frac{\theta^2}{2\pi\tau^2} e^{-(T_D-\tau_+)^2/2\tau^2-(T_D'-\tau_+)^2/2\tau^2} H(\tau_-),
$$
$$
H(\tau_-) = \iint dt\, dt' |\eta\tilde{\phi}_0^*(t+\tau_-, t'-\tau_-) - (1-\eta)\tilde{\phi}_0^*(t'+\tau_-, t-\tau_-)|^2. \tag{B6}
$$

Here the function $H(\tau_-)$ encodes the HOM interference pattern.

The estimation of the two unknown delays $\tau_\pm$ is bounded by the multiparameter classical Cramér-Rao bound

$$C \geqslant \frac{1}{n}\mathcal{F}^{-1}, \qquad (B7)$$

where the classical Fisher information matrix $\mathcal{F}$ plays a role analogous to the CFI $\mathcal{F}$ used in single-parameter estimation. As discussed in Ref. [13], the elements of $\mathcal{F}$ are related to the probability functions in Eq. (B6) by

$$\mathcal{F}_{ij} = \frac{1}{p_0}\left(\frac{\partial p_0}{\partial \tau_i}\right)\left(\frac{\partial p_0}{\partial \tau_j}\right) + \int T_D \frac{1}{p_1(T_D)}\left(\frac{\partial p_1(T_D)}{\partial \tau_i}\right)$$
$$\times \left(\frac{\partial p_1(T_D)}{\partial \tau_j}\right) + \int T_D \frac{1}{p_2(T_D)}\left(\frac{\partial p_2(T_D)}{\partial \tau_i}\right)\left(\frac{\partial p_2(T_D)}{\partial \tau_j}\right)$$
$$+ \iint T_D T_D' \frac{1}{p_{12}(T_D, T_D')}\left(\frac{\partial p_{12}(T_D, T_D')}{\partial \tau_i}\right)$$
$$\times \left(\frac{\partial p_{12}(T_D, T_D')}{\partial \tau_j}\right). \qquad (B8)$$

In this equation i and j take one of the values $\pm$, analogous to Eqs. (13). From Eq. (B6) we find

$$\mathcal{F}_{++} = O(\tau^{-2}),$$
$$\mathcal{F}_{+-} = O(\tau^{-2}),$$
$$\mathcal{F}_{--} = \frac{\theta^2}{H(\tau_-)}\left(\frac{\partial H(\tau_-)}{\partial \tau_-}\right)^2 + O(\tau^{-1}). \qquad (B9)$$

Though the single-click probabilities p_1 and p_2 contain a two-photon interference signal in the second term, due to the reduced signal contrast, the contribution to the CFI matrix is at a lower order of τ compared to the contribution from the coincidence probability p_{12}. The multiparameter CCRB then bounds the variance of estimates of τ_- by $\langle \Delta^2 \tau_- \rangle \geqslant \mathcal{F}_{--} - \mathcal{F}_{+-}^2/\mathcal{F}_{++}$, similar to Eq. (6) for the multiparameter QCRB. From the matrix elements above, the bound is

$$\langle \Delta^2 \tau_- \rangle \geqslant \frac{\theta^2}{H(\tau_-)}\left(\frac{\partial H(\tau_-)}{\partial \tau_-}\right)^2 + O(\tau^{-1}). \qquad (B10)$$

Identifying $\theta^2 H(\tau_-)$ with the coincidence probability (20), the multiparameter CCRB agrees with the single-parameter bound of Eq. (2) to lowest order in the detector time resolution τ.

In many photodetectors the slow time resolution is due primarily to the electronic response time, rather than being related to some intrinsic detector bandwidth, as was assumed in this model. An electronic time response may be included by convolving the probabilities in Eq. (B6) with an additional Gaussian describing the electronic time response. If the electronic response time is τ_e, then the outcome probabilities of the combined system will have the same form as Eq. (B6) but with the parameter τ replaced by $\sqrt{\tau^2 + \tau_e^2}$. The results of this Appendix are still applicable to this more general situation, with the τ now representing an effective time resolution of both the detector and related electronics.

[1] C. K. Hong, Z. Y. Ou, and L. Mandel, Measurement of Subpicosecond Time Intervals between Two Photons by Interference, Phys. Rev. Lett. **59**, 2044 (1987).

[2] F. Bouchard, A. Sit, Y. Zhang, R. Fickler, F. M. Miatto, Y. Yao, F. Sciarrino, and E. Karimi, Two-photon interference: The Hong-Ou-Mandel effect, Rep. Prog. Phys. **84**, 012402 (2021).

[3] E. Knill, R. Laflamme, and G. J. Milburn, A scheme for efficient quantum computation with linear optics, Nature (London) **409**, 46 (2001).

[4] K. N. Cassemiro, K. Laiho, and C. Silberhorn, Accessing the purity of a single photon by the width of the Hong-Ou-Mandel interference, New J. Phys. **12**, 113052 (2010).

[5] A. M. Steinberg, P. G. Kwiat, and R. Y. Chiao, Measurement of the Single-Photon Tunneling Time, Phys. Rev. Lett. **71**, 708 (1993).

[6] J. G. Rarity and P. R. Tapster, Two-color photons and nonlocality in fourth-order interference, Phys. Rev. A **41**, 5139 (1990).

[7] A. Lyons, G. C. Knee, E. Bolduc, T. Roger, J. Leach, E. M. Gauger, and D. Faccio, Attosecond-resolution Hong-Ou-Mandel interferometry, Sci. Adv. **4**, eaap9416 (2018).

[8] Y. Chen, M. Fink, F. Steinlechner, J. P. Torres, and R. Ursin, Hong-Ou-Mandel interferometry on a biphoton beat note, npj Quantum Inf. **5**, 43 (2019).

[9] M. Parniak, S. Borówka, K. Boroszko, W. Wasilewski, K. Banaszek, and R. Demkowicz-Dobrzański, Beating the Rayleigh Limit Using Two-Photon Interference, Phys. Rev. Lett. **121**, 250503 (2018).

[10] N. Fabre and S. Felicetti, Parameter estimation of time and frequency shifts with generalized Hong-Ou-Mandel interferometry, Phys. Rev. A **104**, 022208 (2021).

[11] A. Nomerotski, M. Keach, P. Stankus, P. Svihra, and S. Vintskevich, Counting of Hong-Ou-Mandel bunched optical photons using a fast pixel camera, Sensors **20**, 3475 (2020).

[12] S. L. Braunstein and C. M. Caves, Statistical Distance and the Geometry of Quantum States, Phys. Rev. Lett. **72**, 3439 (1994).

[13] J. Liu, H. Yuan, X.-M. Lu, and X. Wang, Quantum Fisher information matrix and multiparameter estimation, J. Phys. A: Math. Theor. **53**, 023001 (2020).

[14] C. M. Caves, Quantum-mechanical noise in an interferometer, Phys. Rev. D **23**, 1693 (1981).

[15] J. P. Dowling, Quantum optical metrology—the lowdown on high-N00N states, Contemp. Phys. **49**, 125 (2008).

[16] A. M. Steinberg, P. G. Kwiat, and R. Y. Chiao, Dispersion cancellation and high-resolution time measurements in a fourth-order optical interferometer, Phys. Rev. A **45**, 6659 (1992).

[17] H. Scott, D. Branford, N. Westerberg, J. Leach, and E. M. Gauger, Noise limits on two-photon interferometric sensing, Phys. Rev. A **104**, 053704 (2021).

[18] H. Scott, D. Branford, N. Westerberg, J. Leach, and E. M. Gauger, Beyond coincidence in Hong-Ou-Mandel interferometry, Phys. Rev. A **102**, 033714 (2020).

[19] B. Ndagano, H. Defienne, D. Branford, Y. D. Shah, A. Lyons, N. Westerberg, E. M. Gauger, and D. Faccio, Quantum microscopy based on Hong-Ou-Mandel interference, Nat. Photon. **16**, 384 (2022).

[20] M. Reisner, F. Mazeas, R. Dauliat, B. Leconte, D. Aktas, R. Cannon, P. Roy, R. Jamier, G. Sauder, F. Kaiser, S. Tanzilli, and L. Labonté, Quantum-limited determination of refractive index difference by means of entanglement, npj Quantum Inf. **8**, 58 (2022).

[21] A. F. Abouraddy, M. B. Nasr, B. E. A. Saleh, A. V. Sergienko, and M. C. Teich, Quantum-optical coherence tomography with dispersion cancellation, Phys. Rev. A **65**, 053817 (2002).

[22] Y. Liu, R. Quan, X. Xiang, H. Hong, M. Cao, T. Liu, R. Dong, and S. Zhang, Quantum clock synchronization over 20-km multiple segmented fibers with frequency-correlated photon pairs and HOM interference, Appl. Phys. Lett. **119**, 144003 (2021).

[23] R. W. Boyd, *Nonlinear Optics* (Academic, New York, 2020).

[24] P. J. Mosley, J. S. Lundeen, B. J. Smith, P. Wasylczyk, A. B. U'Ren, C. Silberhorn, and I. A. Walmsley, Heralded Generation of Ultrafast Single Photons in Pure Quantum States, Phys. Rev. Lett. **100**, 133601 (2008).

[25] A. B. U'Ren, K. Banaszek, and I. A. Walmsley, Photon engineering for quantum information processing, Quantum Inf. Comput. **3**, 480 (2003).

[26] T. Gerrits, F. Marsili, V. B. Verma, L. K. Shalm, M. Shaw, R. P. Mirin, and S. W. Nam, Spectral correlation measurements at the Hong-Ou-Mandel interference dip, Phys. Rev. A **91**, 013830 (2015).